Engineering 4 (2018) 772–778

Contents lists available at ScienceDirect

Engineering

journal homepage: www.elsevier.com/locate/eng

Research
Precision Engineering—Review

Dual-Comb Ranging

Zebin Zhu [a], Guanhao Wu [a,b,*]

[a] State Key Laboratory of Precision Measurement Technology and Instruments, Department of Precision Instrument, Tsinghua University, Beijing 100084, China
[b] Division of Advanced Manufacturing, Graduate School at Shenzhen, Tsinghua University, Shenzhen 518055, China

ARTICLE INFO

Article history:
Received 20 April 2018
Revised 20 June 2018
Accepted 19 October 2018
Available online 26 October 2018

Keywords:
Ranging
Dual-comb interferometer
Phase noise
Timing jitter
Tight-locking
Post-correction

ABSTRACT

Absolute distance measurement is a fundamental technique in mobile and large-scale dimensional metrology. Dual-comb ranging is emerging as a powerful tool that exploits phase resolution and frequency accuracy for high-precision and fast-rate distance measurement. Using two coherent frequency combs, dual-comb ranging allows time and phase response to be measured rapidly. It breaks through the limitations related to the responsive bandwidth, ambiguity range, and dynamic measurement characteristics of conventional ranging tools. This review introduces dual-comb ranging and summarizes the key techniques for realizing this ranging tool. As optical frequency comb technology progresses, dual-comb ranging shows promise for various professional applications.

1. Introduction

A precise and fast distance-measurement method is necessary in mobile and large-scale dimensional metrology [1,2]. In traditional distance-measurement methods, such as the homodyne or heterodyne methods, a continuous wavelength (CW) laser is used to measure distance or length by accumulating the interferometric phase to achieve a high precision [3]; these methods have been applied in gravitational-wave strain [4]. However, the ambiguity range of this kind of single-wavelength interferometer is only half the wavelength of the used wavelength, and phase accumulation must be consecutive to avoid interruption during measurement. In contrast, light detection and ranging (LIDAR) allows interruption along the beam path and measures distance through pulsed or radio frequency (RF)-modulated waveforms. Although it has a large ambiguity range, the resolution is usually worse than tens of microns. The advent of the optical frequency comb (OFC) as a light source has led to revolutionary progress in ranging and other metrology applications [5–7]. A stable OFC provides narrow-linewidth spectral lines, which serve as a series of CW lasers spaced evenly in the frequency domain. In addition, a stable OFC can potentially accomplish fast measurements due to its repetition rate of hundreds of megahertz, or higher.

Numerous OFC-based ranging systems have been proposed, such as the time-of-flight (TOF) method, which is based on an optical cross-correlation technique [8]; synthetic-wavelength interferometry, which utilizes different optical modes to generate harmonics of an OFC's repetition rate [9–11] or employs multiple wavelengths referenced to a fully stabilized comb [12,13]; and dispersive interferometry, which involves calculating the phase-frequency slope of the interference spectrum [14–16]. These single-comb-based methods realize absolute distance measurement with certain precision and a relatively simple setup. However, they have not fully leveraged all comb modes, as it is often difficult to distinguish adjacent comb lines with megahertz-to-gigahertz mode spacing. Therefore, these single-comb-based ranging methods do not combine the advantages of an OFC, which includes high spectral resolution, fast pulse rate, and large ambiguity range. The dual-comb-based ranging (DCR) system solves this problem by using two OFCs with slightly different repetition rates to realize multi-heterodyne spectroscopy and time-resolved interferograms (IGMs) on a comb tooth-by-tooth basis [17]. In other words, the DCR system utilizes about 10^4 narrow spectral lines to measure distance simultaneously. This dual-comb-based concept provides a unique combination of high precision, high speed, and a large ambiguity range, and has been widely used in absolute distance measurement [18–34]. Although this paper focuses on a dual-comb system applied to distance measurement, the same basic technique has been applied to spectroscopy [35–49], dispersion analysis in long fibers [50], ellipsometry [51], material

* Corresponding author.
E-mail address: guanhaowu@mail.tsinghua.edu.cn (G. Wu).

https://doi.org/10.1016/j.eng.2018.10.002

characterization [52], hyperspectral imaging [53–55], microscopy [56,57], vibrometry [32], and strain sensors [58]. These applications highlight the versatility of the dual-comb system; they have the same underlying dual-comb architecture and confront similar technical challenges [46–49,59–64].

This review is organized as follows: Section 2 provides a basic introduction to TOF-based DCR, including the principles of the system and parameter optimization. To address higher precision, Section 3 introduces synthetic-wavelength interferometry (SWI) and carrier-wave interferometry (CWI) in a DCR system in the absence of phase noise and intensity noise. Actual DCR system must contend with finite linewidths, comb drift, and intensity fluctuations. Section 4 discusses these noise sources and corresponding methods to realize a low-noise DCR. Section 5 concludes by summarizing current progress and future challenges.

2. TOF-based DCR

2.1. Interferograms in time and frequency domains

An OFC is a broadband coherent light source consisting of a series of discrete longitudinal optical modes. Each optical mode can be described in terms of repetition rate (f_r) and offset frequency (f_o) as $f(n) = nf_r + f_o$ [5,6]. The dual-comb system uses a pair of combs with a slight repetition rate difference; this is also known as linear optical sampling in the time domain and multi-heterodyne spectroscopy in the frequency domain.

Fig. 1 shows the DCR system. A pulse train from the signal laser (Comb 1, repetition rate f_{r1}, repetition time T_{r1}) passes through a Michelson interferometer, generating two pulse trains separated by reflections from the measurement (M) and reference (R) mirrors. Next, the local oscillator (LO) laser (Comb 2, repetition rate f_{r2}, repetition time T_{r2}), beats with the signal laser. The two combs have a slight repetition rate difference of $\Delta f_r = f_{r1} - f_{r2}$. The light is filtered with an optical spectrum width of $\Delta\upsilon_{comb}$. The detected signal is filtered via a low-pass electronic filter and then digitized and processed. The IGMs are depicted as periodic envelopes multiplied by a carrier wave signal, as illustrated in the time domain and frequency domain.

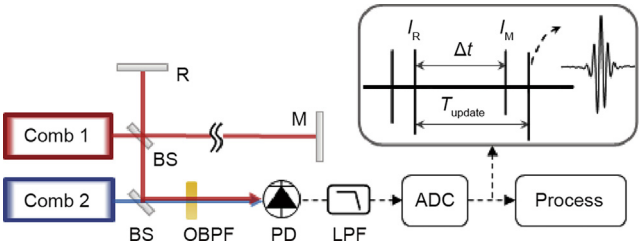

Fig. 1. Simplified image of a DCR system. The pulse train from a signal laser (Comb 1) passes through the Michelson interferometer and then combines with an LO laser (Comb 2). Depending on the configuration, a tunable bandpass filter is employed to satisfy the Nyquist condition. The sampling clock is usually equal to f_{r2}. BS: beam splitter; OBPF: optical bandpass filter; PD: photoelectric detector; LPF: low-pass filter; T_{update}: update time; I_R: reference interferograms; I_M: measurement interferograms; Δt: measured time delay; ADC: analog-to-digital converter.

The time-domain description of a DCR system is shown in Fig. 2. Two separate pulse trains with a time delay of $\Delta\tau$ are sampled linearly by the pulse train from Comb 2 with an effective time step as follows:

$$\Delta T = |T_{r1} - T_{r2}| = \frac{\Delta f_r}{f_{r1} f_{r2}} \tag{1}$$

This generates IGMs (I_R and I_M) with a certain update time, $T_{update} = m \cdot T_{r1} = 1/\Delta f_r$, where $m = f_{r1}/\Delta f_r$ and denotes the number of measurement pulses in every T_{update}. The Nyquist sampling limitation requires the optical bandwidth of the combs to satisfy the relationship $\Delta\upsilon_{comb} < 1/(2\Delta T)$. As a result, the measured time delay is amplified as follows: $\Delta t = m \cdot \Delta\tau$, where Δt is determined by the peaks of the fitted envelopes [19,65]. The distance can be obtained from this TOF information (D_{TOF}), expressed as follows:

$$D_{TOF} = \frac{\upsilon \Delta t}{2} \cdot \frac{\Delta f_r}{f_{r1}} \tag{2}$$

where υ is the optical pulse velocity.

In the frequency domain, we can consider the DCR system as a multi-heterodyne spectrometer with massively parallel CW lasers; its output is simply an RF comb, as shown in Fig. 3. The intensity and phase of the detected RF comb teeth are proportional to the product of the electric fields of the two combs. To ensure a one-to-one mapping of the optical modes to the RF modes, it is necessary for $\Delta\upsilon_{comb} < mf_{r2}/2$, where m also denotes the number of modes of Comb 2 for every period in the frequency domain. Thus, the DCR system should strictly satisfy the following condition:

$$\Delta\upsilon_{comb} < \frac{f_{r1} f_{r2}}{2\Delta f_r} \tag{3}$$

which is equivalent to the Nyquist sampling limitation in the time-domain description. The DCR system generates two RF combs, as depicted above, because the signal-pulse train is divided into two; the main difference between them is the phase spectrum (φ_R for I_R and φ_M for I_M). If we regard the DCR system as dispersive interferometry [14], then the TOF information can also be obtained from

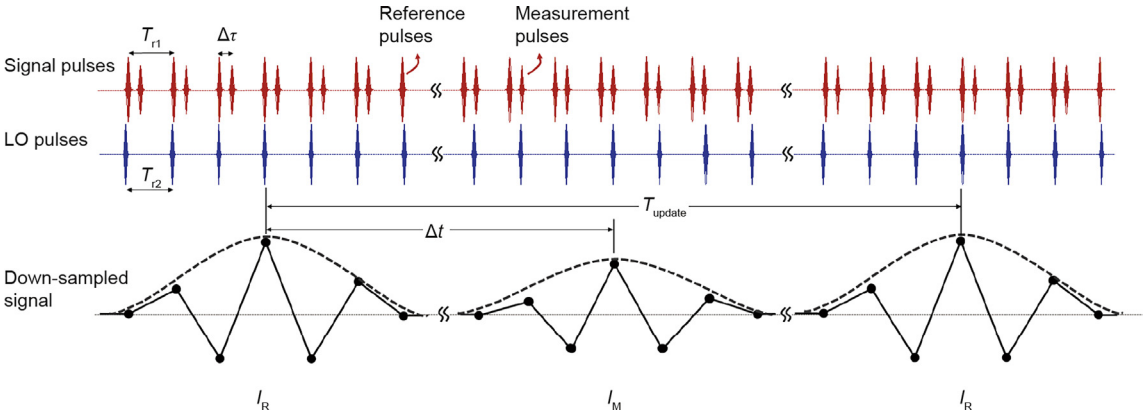

Fig. 2. Time-domain description of the DCR system. The signal and LO emit pulse trains with different repetition rates; the relative timing between the signal and the LO pulse proceeds in increments of ΔT with each sequential pulse. As a result, the measured time delay $\Delta\tau$ is scaled up to Δt.

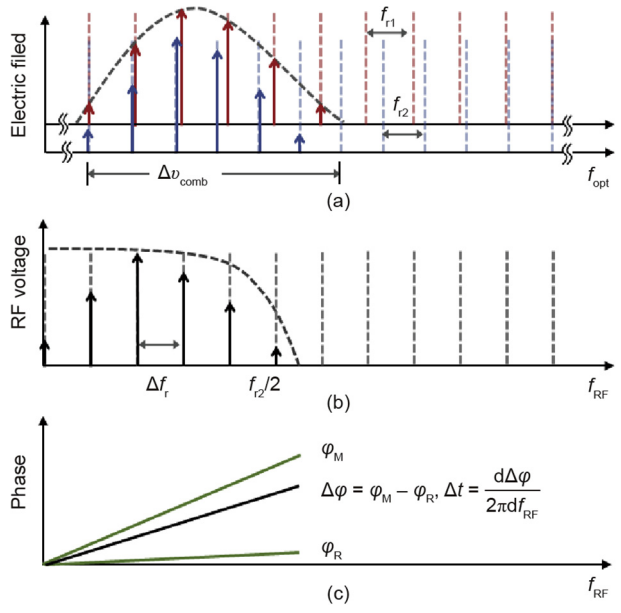

Fig. 3. Frequency-domain description of the DCR system. (a) The description of two OFCs; (b) the description of RF comb; (c) the phase information of the RF comb. In (a) and (b), the solid dashed curves indicate the OBPF and electronic LPF applied in the optical and RF domain, respectively. The straight dashed lines indicate the optical comb lines and RF comb lines before using the OBPF and electronic LPF, respectively. f_{opt}: optical frequency; f_{RF} is the radio frequency.

the phase-frequency slope as follows: $\Delta t = d\Delta\varphi/(2\pi df_{RF})$, where $\Delta\varphi = \varphi_M - \varphi_R$; f_{RF} is the radio frequency. A detailed demonstration is presented in Section 3.

2.2. Parameter optimization

The parameters of the two combs exert a significant impact on the precision of the TOF-based DCR [19,22,24]. A basic condition is that the RF spectrum should be located between 0 and $f_{r2}/2$, as displayed in Fig. 3. According to the Nyquist condition (Eq. (3)), a smaller Δf_r is preferred to avoid aliasing when f_{r1}, f_{r2}, and $\Delta\upsilon_{comb}$ are maintained. Meanwhile, a larger factor of $m = f_{r1}/\Delta f_r$ benefits the low timing jitter ($\Delta\tau = \Delta t/m$); however, the uncertainty analysis of Eq. (2) leads to an opposite result. For simplicity, the D_{TOF} is replaced by D in the relative uncertainty (U_D/D) of TOF-based ranging results, expressed as follows:

$$\begin{aligned}\frac{U_D}{D} &= \sqrt{\left[\frac{\partial(\ln D)}{\partial\upsilon}\right]^2 u_\upsilon^2 + \left[\frac{\partial(\ln D)}{\partial\Delta t}\right]^2 u_{\Delta t}^2 + \left[\frac{\partial(\ln D)}{\partial\Delta f_r}\right]^2 u_{\Delta f_r}^2 + \left[\frac{\partial(\ln D)}{\partial f_{r1}}\right]^2 u_{f_{r1}}^2} \\ &= \sqrt{\left(\frac{u_\upsilon}{\upsilon}\right)^2 + \left(\frac{u_{\Delta t}}{\Delta t}\right)^2 + \left(\frac{u_{\Delta f_r}}{\Delta f_r}\right)^2 + \left(\frac{u_{f_{r1}}}{f_{r1}}\right)^2} \\ &\approx \sqrt{\left(\frac{u_{\Delta t}}{\Delta t}\right)^2 + \left(\frac{u_{\Delta f_r}}{\Delta f_r}\right)^2 + \left(\frac{u_{f_{r1}}}{f_{r1}}\right)^2}\end{aligned} \tag{4}$$

First, we ignore the pulse velocity uncertainty caused by environmental disturbance; only three parts remain—the uncertainties of $_{\Delta}t$, Δf_r, and f_{r1} (denoted as $u_{\Delta t}$, $u_{\Delta f_r}$, and $u_{f_{r1}}$). Clearly, a larger Δf_r will decrease the relative uncertainty. Therefore, an optimal Δf_r region should be chosen for TOF-based DCR, as has been demonstrated in experiments and simulations [19,22]. Moreover, the optimal region varies among DCR systems under different degrees of uncertainty.

Second, we prefer a high repetition rate to reduce $u_{f_{r1}}/f_{r1}$ and $u_{\Delta f_r}/\Delta f_r$ because we can choose a larger Δf_r if high-repetition-rate combs are available. Therefore, we can improve the ranging precision and measurement rate simultaneously. However, a tradeoff exists between precision, measurement rate, and an ambiguity range equals to $\upsilon/(2f_{r1})$. High-repetition-rate DCR systems realized by dissipative Kerr soliton (DKS) states in micro-resonator frequency combs [30,31] and electro-optic combs [32–34] usually provide an update rate in megahertz and sub-micron TOF precision with an ambiguity range in millimeters.

Third, a simple calculation method reduces the uncertainty of the time delay, Δt [27]; the modified time delay can be expressed as follows:

$$\Delta t' = \frac{\Delta t}{\Delta t_{RR}} T_{update} \tag{5}$$

where Δt_{RR} is the measured time delay between two successive reference IGMs. The common uncertainties of Δt and Δt_{RR} are partially removed, thus returning a more stable result.

In summary, the TOF-based DCR can be optimized by adjusting the repetition rate difference, repetition rate, and time-delay calculation method. The precision of TOF results can generally be enhanced to several microns, although results are limited by the intensity noise, to be discussed in Section 4. Regardless of whether intensity noise exists, the precision can be further improved by the application of interferometry in DCR system; see Section 3 for details.

3. Precision enhancement: Interferometry in DCR

3.1. Comb phase information

Fig. 3 shows the frequency-domain principle of DCR, where the phase-frequency slope can be utilized to calculate time delay. In addition, it is possible to obtain a stable phase in all modes. The electric fields of Comb 1 ($E_{R(M)}$, including reference and measurement pulses) and Comb 2 (E_{LO}, LO pulses) are expressed as follows:

$$\begin{aligned}E_{R(M)}(n_1) &= A(n_1)\exp\left\{i[2\pi f_1(n_1) - \varphi_{R(M)}(n_1)]\right\} \\ E_{LO}(n_2) &= A(n_2)\exp\left\{i[2\pi f_2(n_2) - \varphi_{LO}(n_2)]\right\}\end{aligned} \tag{6}$$

where $f_1(n_1)$ and $f_2(n_2)$ represent the frequency modes of Combs 1 and 2, respectively; $A(n_1)$ and $A(n_2)$ are their amplitude, respectively; i is the imaginary symbol. Interference between two electric fields generates reference and measurement IGMs of the following:

$$\begin{aligned}I_{R(M)}(k) &= E_{R(M)}(n_1)E_{LO}^*(n_2) \\ &= I(k)\exp\left\{i[2\pi f_{RF}(k) - \varphi_{R(M)}(k) + \varphi_{LO}(k)]\right\}\end{aligned} \tag{7}$$

where k represents the order of the RF comb mode generated from $E_{R(M)}(n1)$ and E_{LO} $(n2)$; $f_{RF}(k) = f_1(n_1) - f_2(n_2)$; * represents for the conjugate complex number. Next, we can calculate the phase difference $\Delta\varphi(n_1) = \varphi_M(n_1) - \varphi_R(n_1)$ from the RF signal:

$$\begin{aligned}\Delta\varphi(n_1) &= \Delta\varphi(k) = [\varphi_M(k) - \varphi_{LO}(k)] - [\varphi_R(k) - \varphi_{LO}(k)] \\ &= \varphi_M(k) - \varphi_R(k)\end{aligned} \tag{8}$$

Other interferometry can also feasibly be applied, as described below.

3.2. Synthetic-wavelength interferometry

SWI is an effective bridge ranging approach to improve ranging precision. It has an adjustable ambiguity range and a relatively higher precision than the TOF method; thus, it has been widely applied in single-comb ranging methods [9–13]. Given that the DCR system is a mode-resolved interferometer, it is possible to utilize two modes to build a synthetic wavelength (λ_{syn}), expressed as follows:

$$\lambda_{syn} = \frac{\lambda_1 \lambda_2}{\lambda_1 - \lambda_2} \tag{9}$$

where λ_1 and λ_2 are the wavelengths of two modes with phase $\Delta\varphi_1$ and $\Delta\varphi_2$, respectively. The phase of the synthetic wavelength is $\varphi_{syn} = \Delta\varphi_2 - \Delta\varphi_1$. To address the limited measured optical bandwidth, as shown in Eq. (3), two optical bandpass filters with a different center wavelength can be used to extend the range of the wavelength difference [18]. Thus, a more precise result (D_{syn}) can be measured using the synthetic wavelength and its phase, expressed as follows:

$$D_{syn} = \left(N_{syn} + \frac{\varphi_{syn}}{2\pi}\right)\frac{\lambda_{syn}}{2} \tag{10}$$

where N_{syn} is an integer determined by the TOF result D_{TOF}, expressed as follows:

$$N_{syn} = \mathrm{INT}(2D_{TOF}/\lambda_{syn}) \tag{11}$$

where INT represents the integer conversion identifier. The synthetic wavelength is usually dozens of microns, which can be directly linked with TOF-based results. The precision of the SWI-based ranging result reaches about 1 μm.

3.3. Carrier-wave interferometry

CWI, an extremely precise interferometry, is also applied to DCR system. The principle is the same as a single-wavelength light with a Michelson interferometer that measures distance or length. Instead of accumulating the interferometric phase, the SWI-based ranging result D_{syn} is used to determine the multiple integers N_c of the half-carrier wavelength $\lambda_c/2$. In this process, the SWI results should be averaged until the precision is below $\lambda_c/4$. The multiple integer N_c can be expressed as follows:

$$N_c = \mathrm{INT}(2D_{syn}/\lambda_c) \tag{12}$$

Finally, an extremely precise result (D_c) can be calculated by the CWI method, as follows:

$$D_c = \left(N_c + \frac{\varphi_c}{2\pi}\right)\frac{\lambda_c}{2} \tag{13}$$

where φ_c is the interferometric phase of the carrier wavelength λ_c; either $\Delta\varphi_1$ and λ_1 or $\Delta\varphi_2$ and λ_2 can be used.

The process of applying interferometry in DCR system is shown in Fig. 4 [18]. If the measured distance is larger than the ambiguity range of the TOF method ($\upsilon/(2f_{r1})$), other methods will be needed to determine an approximate distance value, such as building a synthetic ambiguity range $\upsilon/(2\Delta f_r)$ that reaches about 10 km by changing the comb repetition rate [17,21].

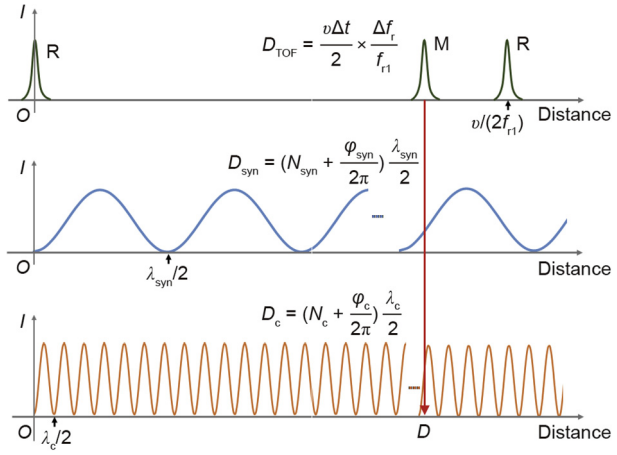

Fig. 4. A combination of TOF, SWI, and CWI methods (three waveforms versus distance).

In summary, the DCR system is a powerful ranging tool for the application of a serial ranging method using a smaller hardware increment. The essential requirement for a DCR system is phase information availability, which is difficult to achieve. In the next section, we discuss phase noise and other noises in a DCR system and introduce a current solution for suppressing noise.

4. Noise analysis and solutions

4.1. Frequency noise, phase noise, and timing jitter

As noted above, a dual-comb interferometer essentially generates an RF comb from an optical comb; therefore, research on the noise of a mode-lock laser is applicable to a dual-comb system [66–69]. In this review paper, we focus on the appearance rather than on the physical essence of laser noise, which enriches our understanding of the tight-locking method and post-correction method.

The repetition rate of an OFC is determined by the equivalent cavity length using $f_r = \upsilon/L$, where L is the cavity length. For simplicity, real-time environmental disturbance induces a relative cavity length change of δL. The instantaneous noise of the repetition rate is $\delta f_r(t) = -f_r(\delta L/L)$, where δL and δf_r represent the noise of corresponding variables. The corresponding phase noise is

$$\delta\varphi_r(t) = \int_0^t \delta f_r(\tau)\mathrm{d}\tau \tag{14}$$

where τ is integral time; t represents the real time. In addition, the timing jitter of pulses is

$$t_{jitter} = \frac{\delta\varphi_r(t)}{2\pi f_r} \tag{15}$$

In a DCR system, we assume that the phase noise of two combs is combined. As the repetition rate of the RF comb is Δf_r, the timing jitter of IGMs in the DCR system (T_{jitter}) is

$$T_{jitter} = \frac{\delta\varphi_r(t)}{2\pi\Delta f_r} \tag{16}$$

We can measure the timing jitter directly in the time domain, for example by using a balanced optical cross-correlator method [66]. Given the complexity of this approach, an optical heterodyne method is more suitable for use with a dual-comb interferometer [60,70]. The relative phase noise between two comb lines can also be measured; this principle is illustrated in Fig. 5. A CW laser is used as an optical intermediary to obtain a relative beat, $f_b = f_1 - f_2$. In this case, two combs are fully stabilized to an RF standard to avoid parameter drift, thus allowing for accurate noise measurement. In free-running case, two CW lasers with separated wavelength are needed to distinguish the noise of f_o and f_r [60,61]. Calculating the instantaneous frequency noise ($\delta f_b(t)$) of the relative beat is simple. Similar to Eq. (14), the phase noise between two combs' modes is $\delta\varphi_b(t)$, from which $\delta\varphi_r(t) = \delta\varphi_b(t)/n_1$ can be determined. Note that $n_1 \approx n_2$ if the Δf_r is not overly large. Finally, the frequency noise, phase noise, and timing jitter of the DCR system can be measured.

Typically, the linewidth of the relative beat f_b reaches about 100 kHz with an approximately 10^4 rad phase fluctuation, and leads to a timing jitter of about 100 ns for IGMs in a fiber-comb-based DCR [60]. The linewidth is much wider than the spacing of the RF comb (Δf_r), and the phase noise is much larger than 2π. Even for unconventional light-source-based DCR systems with inherent

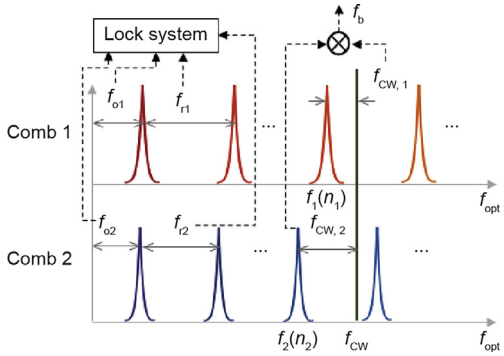

Fig. 5. The principle to generate relative phase noise between two comb lines. Two beat signals between the CW laser and two combs are $f_{CW,1} = f_{CW} - f_1(n_1)$, $f_{CW,2} = f_{CW} - f_2(n_2)$, and $f_b = f_1(n_1) - f_2(n_2)$.

high mutual coherence, such as free-running mode-locked bidirectional dual-comb ring lasers [26,71,72] and electro-optic combs modulated from a single CW laser [32–34,73], a resolved phase has not been achieved. Therefore, noise-suppression methods are required to realize a precise DCR system, as described above.

4.2. Tight-locking method

The conventional approach employs two ultra-stable CW lasers as extremely accurate optical references to stabilize f_o and f_r [17,37,42]. When f_o is phase locked by an f–$2f$ interferometer, only one ultra-stable CW laser is enough [51]. Taking Comb 1 in Fig. 5 as an example, the f_{o1} and $f_{CW,1}$ should be stabilized; a stable repetition rate will be obtained if the CW laser is referenced to an external ultra-stable cavity. Because high mutual coherence is required in a dual-comb interferometer, an electro-optic modulator-based synchronous locking approach is proposed as an alternative. Specifically, one can either lock f_{o1}, f_{o2}, f_{r1}, $f_{CW,1}$, and $f_{CW,2}$ [46] or lock f_{o1}, f_{o2}, f_{r1}, and f_b [18,62]. A feedforward relative stabilization [63] is proposed under a similar principle based on an acousto-optic frequency shifter and piezoelectric transducer (PZT). These tight-locking approaches provide a mode-resolved and phase-stable spectrum; however, the high complexity and cost of tight-locking two combs result in extensive challenges for future applications.

4.3. Post-correction method

The other approach is called the post-correction method; it continuously monitors parameter fluctuations between the two combs and compensates for the noise of dual-comb IGMs instead of feeding back to the comb sources. Two effective post-correction methods, which are realized via analog signal processing [48,74] and digital signal correction [47,49,61], share the same principle: both use two free-running CW lasers with a separated wavelength as optical intermediaries and obtain two relative beat signals between two combs. These two relative beat signals are enough to characterize the noise of the relative offset frequency and relative repetition rate. It is possible to correct the RF comb's offset frequency noise because all modes share the same offset frequency. In addition, the difference between two relative beat signals is irrelevant to the f_o noise, which can be used to correct the Δf_r noise by reconstructing the IGMs' time-domain sampling sequence. It would be much simpler if the post-correction were applied to a high-repetition-rate dual-comb system [59], because the two beat signals are obtained directly from the RF comb. Furthermore, even self-corrected spectroscopy can be realized when two combs initially possess high mutual coherence [75]. This suppresses the relative frequency noise between the two combs, which is sufficient to realize mode-resolved spectroscopy.

Stable phase information is also necessary in the DCR system, but has not yet been demonstrated in existing work. In our recent work, we proposed a digital correction method to realize a mode-resolved and phase-stable dual-comb interferometer [60,64]. We focused on the phase noise of the carrier wave and timing jitter of the IGMs, where the carrier phase noise is computed from the relative beat f_b (Fig. 5), expressed as $\delta\varphi_c(t) = \delta\varphi_b(t) \cdot (f_c/f_{CW})$. The correction algorithm is realized in the time domain and divided into two steps:

First, we simply correct the carrier phase noise:

$$I_1(t) = I_0(t)\exp[-i\delta\varphi_c(t)] \tag{17}$$

where I_0 is the raw IGM; I_1 is the phase-corrected IGM.

Then, we shift the IGMs to compensate for the timing jitter and obtain the phase-timing corrected IGM I_2 as:

$$I_2(t) = I_1\left[t - T_{jitter}(t)\right]\exp\left[-i2\pi f_c T_{jitter}(t)\right] \tag{18}$$

Finally, we obtain the sub-hertz relative linewidth, a relative timing jitter of about 1 ns, and a 0.2 rad precision in the carrier phase. The post-corrected dual-comb system avoids the experimental challenges associated with high-bandwidth active feedback or feedforward. Furthermore, the digital method economizes some of the RF electronics used in analog adaptive sampling. It is also more powerful, since it can manipulate the noise in digital form and take advantage of modern field-programmable gate arrays.

4.4. Intensity noise

In addition to the noises introduced above, intensity noise may affect DCR performance. We demonstrate this phenomenon via a simulation that changes the signal-to-noise ratio (SNR) of an IGM in the time domain and estimates its timing jitter and carrier phase jitter. Fig. 6 shows the results when the SNR ranges from 10 to 10^3. The carrier phase jitter $\delta\varphi_c \propto$ SNR caused by the intensity noise is negligible and can be ignored in most cases because the phase jitter is still about 0.1 rad even with a tight-locking [18] or post-correction method [60]. However, the SNR appears to exert a substantial effect on the timing jitter; the simulation revealed a ~1 ns timing jitter when SNR = 40, which concurred with our experimental results [62]. The simulation results also indicated that it is reasonable to maintain the SNR beyond 20. For low-SNR situations, coherent averaging can suppress intensity noise efficiently as SNR $\propto T^{1/2}$, where T is the coherent averaging time [37,76]. Moreover, when acquiring DCR data over times greater than a few seconds, coherent averaging solves the problem of data

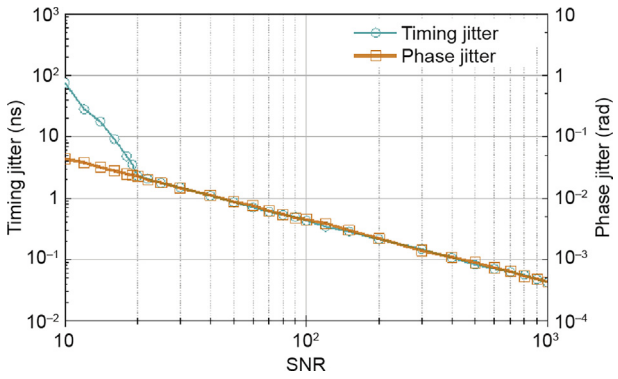

Fig. 6. Relationship between timing jitter, phase jitter, and SNR, estimated by a simulation.

overload because it averages IGMs directly in the time domain. Two conditions should be satisfied here: First, the repetition rates of both combs and the difference between their f_o frequencies should be integer multiples of Δf_r; second, the carrier phase should be sufficiently stable, which can be realized by the tight-locking method and post-correction method. We utilize the exact value of the carrier phase as determined by the measured distance; therefore, we cannot manually adjust the carrier phase to meet the coherent averaging condition.

5. Conclusion

In conclusion, an OFC is an ideal source of absolute distance measurement, as it provides fast pulses and a series of discrete optical modes with broad bands. The DCR system fully exploits these properties to measure distance with high precision, a fast rate, and a long ambiguity range. With the development of OFCs, the DCR system will become a flexible, compact tool with the potential to replace traditional ranging tools in laboratory and field applications. A common concern regarding the air refractive index [77] should be considered in DCR in future. In addition, the DCR system could be further combined with other applications that require both optical amplitude and phase information, such as three-dimensional imaging applications [53–57].

Acknowledgements

This work was supported by the National Natural Science Foundation of China (61575105, 61611140125), Beijing Natural Science Foundation (3182011), and Shenzhen Fundamental Research Funding (JCYJ20170412171535171).

Compliance with ethics guidelines

Zebin Zhu and Guanhao Wu declare that they have no conflict of interest or financial conflicts to disclose.

References

[1] Cuypers W, Van Gestel N, Voet A, Kruth JP, Mingneau J, Bleys P. Optical measurement techniques for mobile and large-scale dimensional metrology. Opt Lasers Eng 2009;47(3–4):292–300.
[2] Schmitt RH, Peterek M, Morse E, Knapp W, Galetto M, Härtig F, et al. Advances in large-scale metrology-review and future trends. Cirp Ann-Manuf Techn 2016;65(2):643–65.
[3] Bobroff N. Recent advances in displacement measuring interferometry. Meas Sci Technol 1993;4(9):907–26.
[4] Abbott BP. Observation of gravitational waves from a binary black hole merger. Phys Rev Lett 2016;116:061102.
[5] Newbury NR. Searching for applications with a fine-tooth comb. Nat Photon 2011;5(4):186–8.
[6] Udem T, Holzwarth R, Hansch TW. Optical frequency metrology. Nature 2002;416(6877):233–7.
[7] Jang YS, Kim SW. Distance measurements using mode-locked lasers: a review. Nanomanu Metrol 2018;1(3):131–47.
[8] Lee J, Kim YJ, Lee K, Lee S, Kim SW. Time-of-flight measurement with femtosecond light pulses. Nat Photon 2010;4(10):716–20.
[9] Minoshima K, Matsumoto H. High-accuracy measurement of 240-m distance in an optical tunnel by use of a compact femtosecond laser. Appl Opt 2000;39 (30):5512–7.
[10] Doloca NR, Meiners-Hagen K, Wedde M, Pollinger F, Abou-Zeid A. Absolute distance measurement system using a femtosecond laser as a modulator. Meas Sci Technol 2010;21(11):115302.
[11] Wu G, Takahashi M, Inaba H, Minoshima K. Pulse-to-pulse alignment technique based on synthetic-wavelength interferometry of optical frequency combs for distance measurement. Opt Lett 2013;38(12):2140–3.
[12] Wang G, Jang YS, Hyun S, Chun BJ, Kang HJ, Yan S, et al. Absolute positioning by multi-wavelength interferometry referenced to the frequency comb of a femtosecond laser. Opt Express 2015;23(7):9121–9.
[13] Jang YS, Wang G, Hyun S, Kang HJ, Chun BJ, Kim YJ, et al. Comb-referenced laser distance interferometer for industrial nanotechnology. Sci Rep 2016;6(1): 31770.
[14] Joo KN, Kim SW. Absolute distance measurement by dispersive interferometry using a femtosecond pulse laser. Opt Express 2006;14(13):5954–60.
[15] Joo KN, Kim Y, Kim SW. Distance measurements by combined method based on a femtosecond pulse laser. Opt Express 2008;16(24):19799–806.
[16] Van den Berg SA, Persijn ST, Kok GJP, Zeitouny MG, Bhattacharya N. Many-wavelength interferometry with thousands of lasers for absolute distance measurement. Phys Rev Lett 2012;108(18):183901.
[17] Coddington I, Swann WC, Nenadovic L, Newbury NR. Rapid and precise absolute distance measurements at long range. Nat Photonics 2009;3(6):351–6.
[18] Zhu Z, Xu G, Ni K, Zhou Q, Wu G. Synthetic-wavelength-based dual-comb interferometry for fast and precise absolute distance measurement. Opt Express 2018;26(5):5747–57.
[19] Wu G, Zhou Q, Shen L, Ni K, Zeng X, Li Y. Experimental optimization of the repetition rate difference in dual-comb ranging system. Appl Phys Express 2014;7(10):106602.
[20] Li Y, Shi J, Wang Y, Ji R, Liu D, Zhou W. Phase distortion correction in dual-comb ranging system. Meas Sci Technol 2017;28(7):075201.
[21] Lee J, Han S, Lee K, Bae E, Kim S, Lee S, et al. Absolute distance measurement by dual-comb interferometry with adjustable synthetic wavelength. Meas Sci Technol 2013;24(4):045201.
[22] Wu G, Xiong S, Ni K, Zhu Z, Zhou Q. Parameter optimization of a dual-comb ranging system by using a numerical simulation method. Opt Express 2015;23 (25):32044–53.
[23] Shi H, Song Y, Liang F, Xu L, Hu M, Wang C. Effect of timing jitter on time-of-flight distance measurements using dual femtosecond lasers. Opt Express 2015;23(11):14057–69.
[24] Zhang H, Wei H, Wu X, Yang H, Li Y. Absolute distance measurement by dual-comb nonlinear asynchronous optical sampling. Opt Express 2014;22(6): 6597–604.
[25] Zhang H, Wei H, Wu X, Yang H, Li Y. Reliable non-ambiguity range extension with dual-comb simultaneous operation in absolute distance measurements. Meas Sci Technol 2014;25(12):125201.
[26] Zhao X, Zheng Z, Liu L, Wang Q, Chen H, Liu J. Fast, long-scan-range pump-probe measurement based on asynchronous sampling using a dual-wavelength mode-locked fiber laser. Opt Express 2012;20(23):25584–9.
[27] Liu TA, Newbury NR, Coddington I. Sub-micron absolute distance measurements in sub-millisecond times with dual free-running femtosecond Er fiber-lasers. Opt Express 2011;19(19):18501–9.
[28] Zhang H, Wu X, Wei H, Li Y. Compact dual-comb absolute distance ranging with an electric reference. IEEE Photon J 2015;7:1–8.
[29] Yang R, Pollinger F, Meiners-Hagen K, Krystek M, Tan J, Bosse H. Absolute distance measurement by dual-comb interferometry with multi-channel digital lock-in phase detection. Meas Sci Technol 2015;26(8):084001.
[30] Trocha P, Karpov M, Ganin D, Pfeiffer MHP, Kordts A, Wolf S, et al. Ultrafast optical ranging using microresonator soliton frequency combs. Science 2018;359(6378):887–91.
[31] Weimann C, Lauermann M, Hoeller F, Freude W, Koos C. Silicon photonic integrated circuit for fast and precise dual-comb distance metrology. Opt Express 2017;25(24):30091–104.
[32] Teleanu EL, Duran V, Torres-Company V. Electro-optic dual-comb interferometer for high-speed vibrometry. Opt Express 2017;25(14): 16427–36.
[33] Wu H, Zhao T, Wang Z, Zhang K, Xue B, Li J, et al. Long distance measurement up to 1.2 km by electro-optic dual-comb interferometry. Appl Phys Lett 2017;111(25):251901.
[34] Zhao X, Qu X, Zhang F, Zhao Y, Tang G. Absolute distance measurement by multi-heterodyne interferometry using an electro-optic triple comb. Opt Lett 2018;43(4):807–10.
[35] Coddington I, Newbury N, Swann W. Dual-comb spectroscopy. Optica 2016;3(4):414–26.
[36] Ideguchi T. Dual-comb spectroscopy. Opt Photon News 2017;28(1):32–9.
[37] Coddington I, Swann WC, Newbury NR. Coherent dual-comb spectroscopy at high signal-to-noise ratio. Phys Rev A 2010;82(4):3535–7.
[38] Coddington I, Swann WC, Newbury NR. Time-domain spectroscopy of molecular free-induction decay in the infrared. Opt Lett 2010;35(9):1395–7.
[39] Cossel KC, Waxman EM, Giorgetta FR, Cermak M, Coddington IR, Hesselius D, et al. Open-path dual-comb spectroscopy to an airborne retroreflector. Optica 2017;4(7):724–8.
[40] Link SM, Maas DJHC, Waldburger D, Keller U. Dual-comb spectroscopy of water vapor with a free-running semiconductor disk laser. Science 2017;356 (6343):1164–8.
[41] Baumann E, Giorgetta FR, Swann WC, Zolot AM, Coddington I, Newbury NR. Spectroscopy of the methane Nu(3) band with an accurate midinfrared coherent dual-comb spectrometer. Phys Rev A 2011;84(6):14717–9.
[42] Coddington I, Swann WC, Newbury NR. Coherent multiheterodyne spectroscopy using stabilized optical frequency combs. Phys Rev Lett 2008;100(1):13902–5
[43] Davila-Rodriguez J, Ozawa A, Hansch TW, Udem T. Doppler cooling trapped ions with a UV frequency comb. Phys Rev Lett 2016;116(4):043002.
[44] Meek SA, Hipke A, Guelachvili G, Hänsch TW, Picqué N. Doppler-free fourier transform spectroscopy. Opt Lett 2017;43(1):162–5.
[45] Hsieh YD, Iyonaga Y, Sakaguchi Y, Yokoyama S, Inaba H, Minoshima K, et al. Spectrally interleaved, comb-mode-resolved spectroscopy using swept dual terahertz combs. Sci Rep 2014;4:3816.
[46] Nishiyama A, Yoshida S, Nakajima Y, Sasada H, Nakagawa K, Onae A, et al. Doppler-free dual-comb spectroscopy of Rb using optical-optical double resonance technique. Opt Express 2016;24(22):25894–904.

[47] Roy J, Deschenes JD, Potvin S, Genest J. Continuous real-time correction and averaging for frequency comb interferometry. Opt Express 2012;20(20):21932–9.
[48] Ideguchi T, Poisson A, Guelachvili G, Picque N, Hansch TW. Adaptive real-time dual-comb spectroscopy. Nat Commun 2014;5(1):3375–82.
[49] Ycas G, Giorgetta FR, Baumann E, Coddington I, Herman D, Diddams SA, et al. High-coherence mid-infrared dual-comb spectroscopy spanning 2.6 to 5.2 μm. Nat Photon 2018;12(4):202–8.
[50] Coddington I, Swann WC, Newbury NR. Coherent linear optical sampling at 15 bits of resolution. Opt Lett 2009;34(14):2153–5.
[51] Minamikawa T, Hsieh YD, Shibuya K, Hase E, Kaneoka Y, Okubo S, et al. Dual-comb spectroscopic ellipsometry. Nat Commun 2017;8(1):610–7.
[52] Asahara A, Nishiyama A, Yoshida S, Kondo K, Nakajima Y, Minoshima K. Dual-comb spectroscopy for rapid characterization of complex optical properties of solids. Opt Lett 2016;41(21):4971–4.
[53] Boudreau S, Levasseur S, Perilla C, Roy S, Genest J. Chemical detection with hyperspectral lidar using dual frequency combs. Opt Express 2013;21(6):7411–8.
[54] Shibuya K, Minamikawa T, Mizutani Y, Yamamoto H, Minoshima K, Yasui T, et al. Scan-less hyperspectral dual-comb single-pixel-imaging in both amplitude and phase. Opt Express 2017;25(18):21947–57.
[55] Wang C, Deng Z, Gu C, Liu Y, Luo D, Zhu Z, et al. Line-scan spectrum-encoded imaging by dual-comb interferometry. Opt Lett 2018;43(7):1606–9.
[56] Hase E, Minamikawa T, Mizuno T, Miyamoto S, Ichikawa R, Hsieh YD, et al. Scan-less confocal phase imaging based on dual-comb microscopy. Optica 2018;5(5):634–43.
[57] Dong X, Zhou X, Kang J, Chen L, Lei Z, Zhang C, et al. Ultrafast time-stretch microscopy based on dual-comb asynchronous optical sampling. Opt Lett 2018;43(9):2118–21.
[58] Kuse N, Ozawa A, Kobayashi Y. Static FBG strain sensor with high resolution and large dynamic range by dual-comb spectroscopy. Opt Express 2013;21(9):11141–9.
[59] Burghoff D, Yang Y, Hu Q. Computational multiheterodyne spectroscopy. Sci Adv 2016;2(11):1601227–33.
[60] Zhu Z, Ni K, Zhou Q, Wu G. Digital correction method for realizing a phase-stable dual-comb interferometer. Opt Express 2018;26(13):16813–23.
[61] Deschenes JD, Giaccari P, Genest J. Optical referencing technique with CW lasers as intermediate oscillators for continuous full delay range frequency comb interferometry. Opt Express 2010;18(22):23358–70.
[62] Zhu Z, Xu G, Ni K, Zhou Q, Wu G. Improving the accuracy of a dual-comb interferometer by suppressing the relative linewidth. Meas Sci Technol 2018;29(4):45007–11
[63] Chen Z, Yan M, Hänsch TW, Picqué N. A phase-stable dual-comb interferometer. Nat Commun 2018;9:3035.
[64] Zhu Z, Ni K, Zhou Q, Wu G. A computational correction method for dual-comb interferometry. In: Proceedings of Conference on Lasers and Electro-Optics; 2018 May 13–18; San Jose, CA, USA. California: Optical Society of America; 2018.
[65] Zhang Z, Gu C, Sun J, Wang C, Gardiner T, Reid DT. Asynchronous midinfrared ultrafast optical parametric oscillator for dual-comb spectroscopy. Opt Lett 2012;37(2):187–9.
[66] Kim J, Song Y. Ultralow-noise mode-locked fiber lasers and frequency combs: principles, status, and applications. Adv Opt Photonics 2016;8(3):465.
[67] Ferre-Pikal ES, Vig JR, Camparo JC, Cutler LS, Maleki L, Riley WJ, et al. Draft revision of IEEE STD 1139–1988 standard definitions of physical quantities for fundamental, frequency and time metrology-random instabilities. In: Proceedings of International Frequency Control Symposium; 1997 May 30; Orlando, FL, USA. New York: IEEE; 2002. p. 338–57.
[68] Paschotta R. Noise of mode-locked lasers (part I): numerical model. Appl Phys B 2004;79(2):153–62.
[69] Von Bandel N, Myara M, Sellahi M, Souici T, Dardaillon R, Signoret P. Time-dependent laser linewidth: beat-note digital acquisition and numerical analysis. Opt Express 2016;24(24):27961–78.
[70] Hou D, Lee CC, Yang Z, Schibli TR. Timing jitter characterization of mode-locked lasers with <1 zs/$\sqrt{}$Hz resolution using a simple optical heterodyne technique. Opt Lett 2015;40(13):2985–8.
[71] Ideguchi T, Nakamura T, Kobayashi Y, Goda K. Kerr-lens mode-locked bidirectional dual-comb ring laser for broadband dual-comb spectroscopy. Optica 2016;3(7):748–53.
[72] Liao R, Song Y, Liu W, Shi H, Chai L, Hu M. Dual-comb spectroscopy with a single free-running thulium-doped fiber laser. Opt Express 2018;26(8):11046–54.
[73] Millot G, Pitois S, Yan M, Hovhannisyan T, Bendahmane A, Hänsch TW, et al. Frequency-agile dual-comb spectroscopy. Nat Photon 2016;10(1):27–30.
[74] Ideguchi T, Poisson A, Guelachvili G, Haensch TW, Picque N. Adaptive dual-comb spectroscopy in the green region. Opt Lett 2012;37(23):4847–9.
[75] Hebert NB, Genest J, Deschênes JD, Bergeron H, Chen GY, Khurmi C, et al. Self-corrected chip-based dual-comb spectrometer. Opt Express 2017;25(7):8168–79.
[76] Newbury NR, Coddington I, Swann W. Sensitivity of coherent dual-comb spectroscopy. Opt Express 2010;18(8):7929–45.
[77] Jang YS, Kim SW. Compensation of the refractive index of air in laser interferometer for distance measurement: a review. Int J Precis Eng Manuf 2017;18(12):1881–90.